Soft Matter

Dynamic Article Links ▶

PAPER

Peptide-directed co-assembly of nanoprobes on multimaterial patterned solid surfaces†

Marketa Hnilova, Christopher R. So, E. Emre Oren,‡ Brandon R. Wilson, Turgay Kacar, Candan Tamerler* and Mehmet Sarikaya*

Biocombinatorially selected solid-binding peptides, through their unique material affinity and selectivity, are a promising platform for building up complex hierarchical assemblies of nanoscale materials and molecular probes, targeted to specific practical solid surfaces. Here, we demonstrate the material-specific characteristics of engineered gold-binding and silica-binding peptides through co-assembly onto micro- and nano-patterned gold surfaces on silica substrates. To build hierarchical nanostructures on patterned solid surfaces, we utilize peptides as molecular tools and monitor their behavior by either conjugating biotin to them for specific affinity to streptavidin-coated QDot nanoparticles or labelling them with small fluorescent labels. This biomimetic peptide-based approach could be used as an alternative to conventional chemical coupling and surface functionalization techniques with substantial advantages, allowing simultaneous assembly of two or more inorganic nano-entities and/or molecular probes onto patterned inorganic solid substrates. The results have significant implications in a wide range of potential applications, including controlled assembly of hybrid nanostructures in bionanophotonic and biosensing devices.

Introduction

Hybrid micro- and nano-structures composed of diverse inorganic materials coupled with biomolecules, *e.g.*, proteins and DNA, are of considerable interest for the development of new biosensors, biotechnology protocols, and proteomic devices.[1–6] Recently, emerging 'bottom up' nano-biotechnological applications, *e.g.*, biofabrication, bionanophotonics, and protein/cell immobilization, require highly controlled, selective and efficient biomolecule adsorption onto desired locations of inorganic substrates under biological environments.[7,8] Current approaches for coupling inorganics with biomolecules, or linking two inorganics, predominantly require multiple surface functionalization steps *via* self-assembled monolayers (SAMs), using, *e.g.*, thiols[9,10] or silanes,[11,12] as linkers on either metal or oxide substrates, respectively. In SAMs, functional "head" groups form stable

covalent bonds with the solid surface while long aliphatic "tail" carbon chains and their functional end groups form a dense and chemically tailorable monolayer.[9,10,13] Although used frequently in conventional approaches, both SAM systems may present low coupling efficiencies, biocompatibility and biomolecule stability limitations due to high temperatures, organic solvents and harsh chemicals often required during monolayer preparations and bioconjugation processes.[14–16] There is a need, therefore, to establish material-specific and biocompatible molecular immobilization techniques to realize multi-component bionanotechnology.[17,18]

Recently, an alternative biologically friendly technique has emerged that utilizes solid-binding peptides as molecular linkers for the immobilization of proteins, polymers, and nanoparticles onto solid surfaces.[17–21] Over the last decade, phage display[22] and cell surface display[23,24] approaches have been adopted as powerful strategies for selecting peptides with affinity to various solids.[17–21] So far, peptide sequences which bind to metals (Au,[24–26] Ag,[21] Pt[27]), oxides (ZnO,[28] Cu$_2$O,[28] TiO$_2$,[29] SiO$_2$[30]), and semiconductors (GaN and GaAs[20]) have been identified and demonstrated potential utility in inorganic synthesis[21,31–33] and hierarchical assembly.[34,35] Selected solid-binding peptides are robust molecular linkers that can be further genetically engineered or chemically modified for tailored functionalities, including molecular-binding and -linking to specific solids.[18,29,31] Though promising, using peptides as highly efficient linkers for surface modification and immobilization of inorganic

GEMSEC, Genetically Engineered Materials Science and Engineering Center, Materials Science and Engineering Department, University of Washington, Roberts Hall, Box: 352120, Seattle, WA 98195, USA. E-mail: sarikaya@u.washington.edu; candan@u.washington.edu; Fax: +1 (206) 543-3100; Tel: +1 (206) 543-0724; +1 (206) 616 6980

nanostructures or biologically viable probes onto specific materials remains largely unexplored.

Here, following up our earlier material affinity work,[35] we discover that unique gold- and silica-binding peptide sequences (AuBP and QBP, respectively) exhibit opposite material selective properties for gold and silica. High-affinity AuBPs and QBPs were recently selected through biocombinatorial peptide libraries and tailored through *in silico* design.[25,30] Through designing and utilizing both peptide sequences, we successfully demonstrate the co-assembly of quantum dots (QDots) and fluorescein isothiocyanate (FITC) fluorophore on a shared nanopatterned gold/silica substrate. The described peptide-based fabrication process is highly versatile and biocompatible. Overall, this biomolecular platform could be successfully used for surface functionalization to allow the simultaneous assembly of two or more inorganic and/or organic nano-entities and molecular probes onto desired locations of solid substrates under ambient conditions for the development of nanophotonic and biosensing devices.

Materials and methods

Biocombinatorial selection of gold-binding peptides

The gold-binding peptides were selected from FliTrx bacterial surface library (Invitrogen, USA) displaying randomized dodecapeptides inserted into FLITRX chimera bacterial surface flagellin protein.[36] Clean 99.9% pure Au foils (Goodfellow Corp., USA) were used as a target for novel solid-binding peptide selection. Five selection rounds were applied in the entire panning experiment for the enrichment of gold-binding clones as described elsewhere.[25,28] The binding affinity and material selectivity characteristics of isolated clones were further characterized in fluorescence microscopy experiment; typically, same aliquots of induced cell clones (OD = 0.5) were labeled by 7.5 μM nucleic-acid fluorescent dye SYTO9 (Molecular Probes, USA) and incubated with an Au surface (5 × 5 mm) deposited on glass using a sputter coating system (672 PECS, Gatan, Inc., USA) to the thickness of deposited metal 25 nm for 1 h. After washing step bound cells were visualized on a Nikon TE-2000U Fluorescence Microscope (Nikon, Japan) coupled with Hamamatsu ORCA-ER cooled CCD camera using METAMORPH software (Universal Imaging, USA) and a FITC filter (exciter 460–500, dichroic 505, emitter 510–560; Chroma Technology Co., USA). Material selectivity tests were carried out as described above using a Ag surface (5 × 5 mm) deposited on glass sample or SiO$_2$ wafer instead.

Peptide syntheses and modifications

Material-selective gold-binding peptide AuBP2 (M_w: 1591.8, WALRRSIRRQSY) was synthesized in-house using the *Fmoc* SPPS technique by Bio-Peptide Co., USA. 2 mg of synthesized gold-binding peptide were biotinylated using NSH-biotin reagent (Pierce, USA); molecular mass of biotinylated peptide (AuBP2-bio, M_w: 1819.1) was confirmed by MALDI mass spectroscopy (Bruker Autoflex II, Bruker Daltonics, USA) as shown in the ESI†. *De novo*-designed silica-binding peptide QBP1 (M_w: 1466.0, PPPWLPYMPPWS) was synthesized using

the *Fmoc* SPPS technique and modified with either biotin (QBP1-bio) or FITC (QBP1-FITC) by UBR Co., USA.

Surface plasmon resonance (SPR) binding experiments

SPR measurements were performed using a four channel instrument (Kretschmann configuration) developed by the Radio Engineering Institute, Czech Republic. It was equipped with a polychromatic light source (Ocean Optics LS1). The instrument can detect changes at a level of 0.0001 refractive index unit, and is temperature controlled. Buffer and peptide solutions were degassed to avoid bubbles in the flow cell. First, a phosphate buffer solution (1 : 3 mix of 10 mM KH$_2$PO$_4$, 10 mM K$_2$HPO$_4$ and 100 mM KCl) was flowed over the surface until a stable baseline signal was established. Then, peptide solutions in phosphate buffer at 0.46 μM (AuBP2) or 5 μM (QBP1) concentrations were flowed over the Au or SiO$_2$ surface and peptide adsorption kinetics were monitored. After the surface coverage reached or neared equilibrium, the phosphate buffer solution was flowed again and desorption of the peptide was monitored. The system was then cleaned using a 1% SDS + 0.1 M NaOH solution, followed by a 0.1 M HCl solution, and finally DI water. Unlike the Au surface, silica material does not have a measurable SPR signal. To overcome this difficulty a very thin film (5 nm) of silica was coated onto the Au substrate using the sputter coating system (672 PECS, Gatan, Inc., USA). The coated silica thicknesses were predetermined using a mathematical model developed in our group (unpublished data) and controlled by the calibrated QCM thickness monitor (672 PECS, Gatan, Inc., USA).[30] For data analysis purposes, the SPR signal was calibrated in order to calculate molecules per cm^2 from the surface plasmon wavelength given by the raw data.

Fabrication of micro- and nano-patterned surfaces

Au micro-patterns on a silica surface were prepared as follows: the native oxide of Si wafer was patterned using the photolithography technique followed by deposition *via* sputtering of Cr (10 nm) and Au (25 nm) on the sputter coating system (672 PECS, Gatan, Inc., USA) and subsequent lift-off of the photoresist to form the Au pattern.[35]

Nano-structured surfaces were prepared as per the nanosphere lithography (NSL) technique reported elsewhere.[37] Briefly, glass cover slips were cleaned in a basic piranha solution (5 : 1 : 1 H$_2$O : NH$_4$OH : 30% H$_2$O$_2$) under sonication for 1 h to form a net negatively charged hydrophilic surface. 10 μl of 1.5 μm and 5.0 μm sized colloidal microsphere solutions (Duke Scientific, USA) were drop-coated onto the aforementioned cleaned glass cover slips in order to obtain close-packed assemblies of microspheres for masking. After samples were fully dried in air, they were placed in a precision ion beam sputter coating system (672 PECS, Gatan, Inc., USA) for an Au coating of 25 nm at a rate of ∼10 Å s^{-1}, as monitored by quartz crystal microbalance. Subsequently, metal-coated substrates were immersed in ethanol and sonicated briefly to remove the microsphere mask and reveal the nanopatterned Au structures. Patterned glass surfaces were then rinsed with ethanol thoroughly.

Fluorescence microscopy binding experiments

Synthesized biotinylated peptides (20 µM AuBP2-bio and 100 µM QBP1-bio in PBS buffer) were incubated for 2 h with Au patterns fabricated on the silica substrate prepared by photolithography and NSL techniques, as described above. The immobilized AuBP2-bio or QBP1-bio were incubated with QDots605 functionalized with streptavidin (2 nM) (Invitrogen, USA) for 15 min and visualized on the Nikon TE-2000U Fluorescence Microscope (Nikon Instruments, Japan) using a QDot605 filter (exciter 320–460, dichroic 475, emitter 605/40 nm; Chroma Technology Co., USA). Similarly, *de novo* silica-binding peptide QBP1 modified with FITC (QBP1-FITC; 60 µM) was used, immobilized FITC-modified peptide was then visualized directly using the FITC filter (exciter 460–500, dichroic 505, emitter 510–560; Chroma Technology Co., USA).

Peptide-targeted co-assembly experiment

In peptide-directed co-immobilization, first the biotinylated gold-binding peptide (AuBP2-bio; 20 µM) was incubated with the Au-patterned NSL surface for 1 h, followed by 15 min incubation of streptavidin-modified QDots605 (2 nM) and 1 h incubation of the silica-binding peptide (QBP1-FITC; 60 µM); immobilized peptides were detected from the same spot on the NSL substrate using a fluorescence microscope with appropriate emission filters as described above.

High-resolution atomic force microscopy (AFM)

A Digital Instruments (USA) Multimode Nanoscope IIIa scanning probe microscope, equipped with high frequency Nano-Sensors PPP-NCHR (NanoAndMore USA, USA) non-contact probes with a 42 N m^{-1} spring constant and ~350 kHz resonance frequency, was used to scan the peptide-QDot functionalized surfaces. All imaging was carried out in non-contact mode in air, with 512 × 512 data acquisitions, at a scan speed of 0.8 Hz, at room temperature, under positive N$_2$ pressure with acoustic isolation. Supplier-provided software (Nanoscope V5.3r1, Veeco) was utilized for generating images. Coverage of SA-QDots on both micro-pads and NSL surfaces was determined by comparing the distribution of heights from AFM histograms using SPIP image processing software (Image Metrology, Denmark). First, bare SiO$_2$ and Au surfaces were analyzed for their characteristic height distributions (see ESI†) and then fitted using multiple Gaussian functions. SA-QDots manifest on the histogram as a broad peak ~5–10 nm offset from the bare peak. Coverage is then calculated by taking the area of the fitted SA-QDot curve (Fig. 3d, red) and dividing it by the area of the entire multi-fitted curve (Fig. 3d, blue). SA-QDot surface coverage on rough gold surfaces was calculated by subtracting an estimated bare curve (characteristic by multiple Gaussian function fitting) from the total fitted curve. For SA-QDot coverage quantification on non-planar NSL surfaces, the analysis was first preceded by a background subtraction method (see ESI†).

Results and discussion

We and other groups have demonstrated that original bio-combinatorially selected solid-binding peptide sequences can be engineered to enhance their binding and selective characteristics by producing peptides that contain repetitive binding motifs or mutations of the amino acid sequence.[29,35,39] Also, improved selectivity can be achieved by integrating simple modifications into the biopanning protocol (*e.g.*, counter-selection step, material specificity testing, *etc.*) to isolate peptides with not only high affinity but also high material selectivity.

Here, we screened gold-binding peptides for high affinity and enhanced material selectivity by applying a modified combinatorial selection procedure using the FliTrx bacterial surface library.[25] Prior to synthesizing peptides individually, we evaluated the binding characteristics of AuBP–FliTrx expressing clones to gold surfaces using fluorescence microscopy (FM), and compared binding affinities to other various materials, *e.g.*, silica and silver. Silica and metallic silver are major constituents of various multimaterial devices[2–5] and, thus, were rationally used for initial cross-binding analyses. These preliminary binding assays allowed us to identify AuBP sequences which exhibit desirable binding characteristics towards Au while still displayed on bacterial cells as FliTrx fusion surface proteins (Fig. 1).

We first demonstrate the adhesion of isolated bacterial clones that display high-affinity (AuBP1 and AuBP2) and low-affinity (AuBP30) FliTrx fusion surface proteins towards the Au surface (Fig. 1b). The fluorescence images shown in Fig. 1b and c demonstrate the enhanced gold-binding behaviour of AuBP–FliTrx fusion protein expressing either of the mutants (AuBP1 and AuBP2). The gold-binding characteristics are evidenced by an increased number of surface-adhered cells that appear as fairly uniformly distributed bright rods on a dark background. Moreover, the figure also displays low adhesion of mutant cells expressing AuBP2 onto Ag and silica surfaces (as schematically illustrated in Fig. 1c). In contrast, plasmid-free control GI826 cells did not adhere to any of the tested surfaces. As further evidenced in these figures, AuBP2 displays higher binding affinity
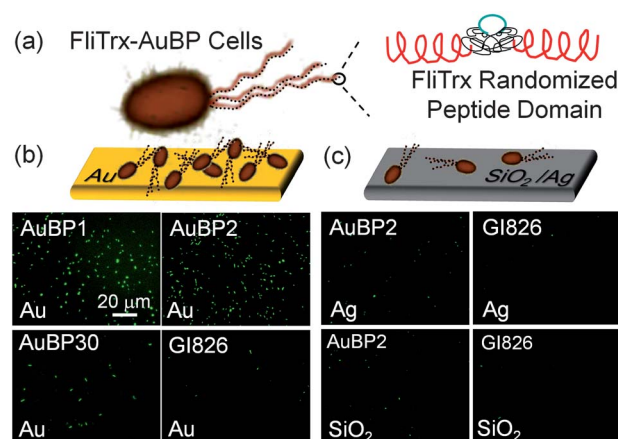

Fig. 1 Material selectivity of selected AuBP–FliTrx bacterial clones. (a) Schematic of FliTrx cell expressing FliTrx–AuBP protein. (b) Gold-adhered FliTrx cells expressing strong (AuBP1, WAGAKRLVLRRE; AuBP2, WALRRSIRRQSY), weak (AuBP30, TLRRWRDRRILN) gold-binding FliTrx protein, and negative control experiment with plasmid free GI826 cells. (c) Material selectivity of strong gold-binding clone (AuBP2) on silver and silica surface with respective plasmid free GI826 control cells. The adhered cells were labeled with nucleic-acid fluorescent SYTO9 dye and visualized using fluorescence microscopy.

(more number of bound cells per area) and material specificity to Au surfaces over AuBP1, making it a better candidate for use in the demonstration of peptide-directed immobilization and surface functionalization, as discussed below.

Successful practical applications of peptide-based biolinkers in nanotechnology require that they retain their substrate affinity and material selectivity when chemically synthesized as peptides, independent of bacterial FliTrx or phage PIII fusion protein partners. Therefore, detailed quantitative binding analysis is required for each synthesized solid-binding peptide to verify their molecular characteristics. As we demonstrate, herein, gold-(AuBP2) and silica-binding (QBP1) peptides are used as specific biological linkers. While the AuBP2 peptide sequence was selected through a modified post-panning procedure as described above, the QBP1 peptide sequence was *in silico* designed using a novel knowledge-based approach generated from the experimental biocombinatorial selection and post-selection binding categorization.[30] Using dynamic programming algorithms, we exploited the information present in the selected peptide sequences and generated novel scoring matrices (*i.e.*, QUARTZ I) that optimize the similarities among the strong silica-binding peptide sequences and the differences between the strong- and weak-binding peptide sequence groups. Subsequently, using the generated scoring matrices we designed novel peptide sequences with enhanced silica-binding affinity and specificity.[30,38] Among the designed peptide sequences, QBP1 is one of the first designed/validated peptides *via* this method.[30,38] Both AuBP2 and QBP1 were previously reported to exhibit excellent binding affinities to their respective materials, *i.e.*, Au and silica, with adsorption parameters roughly corresponding to chemical SAM linker molecules.[19,25,30,38] Specifically, AuBP2 adsorbs to Au surfaces under ambient conditions with an equilibrium constant (K_{eq}) of 2.34×10^6 M^{-1}, corresponding to a binding energy of -8.7 kcal mol^{-1}, as previously detected by surface plasmon resonance (SPR) spectroscopy.[25] The QBP1 sequence binds to various silica surfaces with high affinity in FM as well as in SPR binding experiments.[30,38] The equilibrium constant (K_{eq}) of 0.77×10^6 M^{-1} and respective binding energy of -8 kcal mol^{-1} for QBP1-silica binding were previously determined using a modified SPR technique (unpublished data).

In this work, we further explore the material-selective binding characteristics of AuBP2 and QBP1 with respect to SiO$_2$ and Au surfaces, respectively, using a previously established SPR approach. Specifically, a 5 nm thin film of SiO$_2$ (measured by monitoring the thickness with a quartz crystal microbalance, QCM) was coated onto an Au substrate using a sputter coating system to adapt SPR for the detection of peptide binding to the silica surface.[30,35] Raw kinetic data of AuBP2 (0.46 µM) and QBP1 (5 µM) adsorption onto respective Au and SiO$_2$ surfaces from SPR experiments were fitted with a modified Langmuir adsorption model, reported in detail previously by our group (Fig. 2a).[35,39] The corresponding values of adsorbed peptide mass, per cm^2 after washing step, are plotted in Fig. 2b. As evidenced in the graph from Fig. 2b, tested peptides exhibited significant material recognition and bound preferentially to the surface they were originally selected for, *i.e.*, AuBP2 adsorbed preferentially to Au over silica and QBP1 bound preferentially to silica over the Au surface. It should be emphasized that peptide adsorption was carried out in water-based solvents under physiological pH, therefore, providing biologically viable conditions.
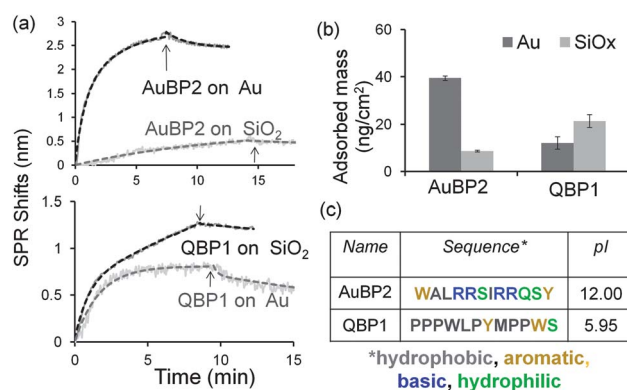

Fig. 2 Binding affinity and material selectivity of AuBP2 and QBP1 *via* SPR. (a) SPR curve fitted with Langmuir profile of 0.46 µM AuBP2 and 5 µM QBP1 on gold and silica surfaces, respectively (arrows indicate buffer only, with no peptide). (b) Quantification of adhered peptide mass per cm^2 calculated from recorded SPR sensorgrams presented in (a). (c) Peptide sequences of AuBP2 and QBP1. The pI values were computed by ProtParam (expasy.com).

To date, the molecular recognition mechanism of peptides binding to solid surfaces has not been fully understood. However, selective peptide binding to inorganic surfaces is likely related to their specific amino acid sequences and the resultant molecular architecture.[18,25,27,30,35,39,40] Here, AuBP2 sequence is rich in polar hydroxyl-containing (S, Y) amino acid residues, which have been previously reported to recognize the Au lattice.[25,26,35,41,42] Most recently, aromatic (Y, F, W) and basic amino acids (R, K) were computationally predicted and experimentally verified to adsorb to Au surfaces with even higher affinity and strength compared to traditional metal-binding amino acids (C, H).[41,43] Thus, the presence of aromatic and basic amino acids (W, Y, R) in AuBP2 potentially implies a novel gold-binding mechanism. At the same time, a lack of individual Cys and His amino acids eliminates the obvious well known metal-binding mechanisms by which peptides can attach non-specifically to metal surfaces.[7,8,11,25,44,45]

In QBP1, on the other hand, hydrophobic amino acids (P) have been reported to be an important constituent for silica-binding peptide sequences[30] and are probably associated with silica binding. By contrast, the present aromatic amino acids (W, Y) may contribute to the observed minor gold-binding characteristics of QBP1. The fact that the tested solid-binding peptides can recognize Au regions over SiO$_2$, and *vice versa*, is of significant practical interest since these peptides can be utilized as specific biological linkers in the simultaneous, selective and spatially controlled immobilization of various nanostructures and molecular probes on the same multimaterial surface, as demonstrated here.

Following the peptide synthesis and quantitative binding experiments with SPR, the peptides were then modified with biotin to display dual functionality. We chose the well-established biotin–streptavidin (bio–SA) molecular coupling because of its low dissociation constant ($\sim 10^{-15}$ M), high reaction speed and stability in a wide range of pH values.[46] We hypothesized that such bifunctional AuBP2-bio and QBP1-bio molecules can direct SA-modified nanostructures, *e.g.*, commercially available
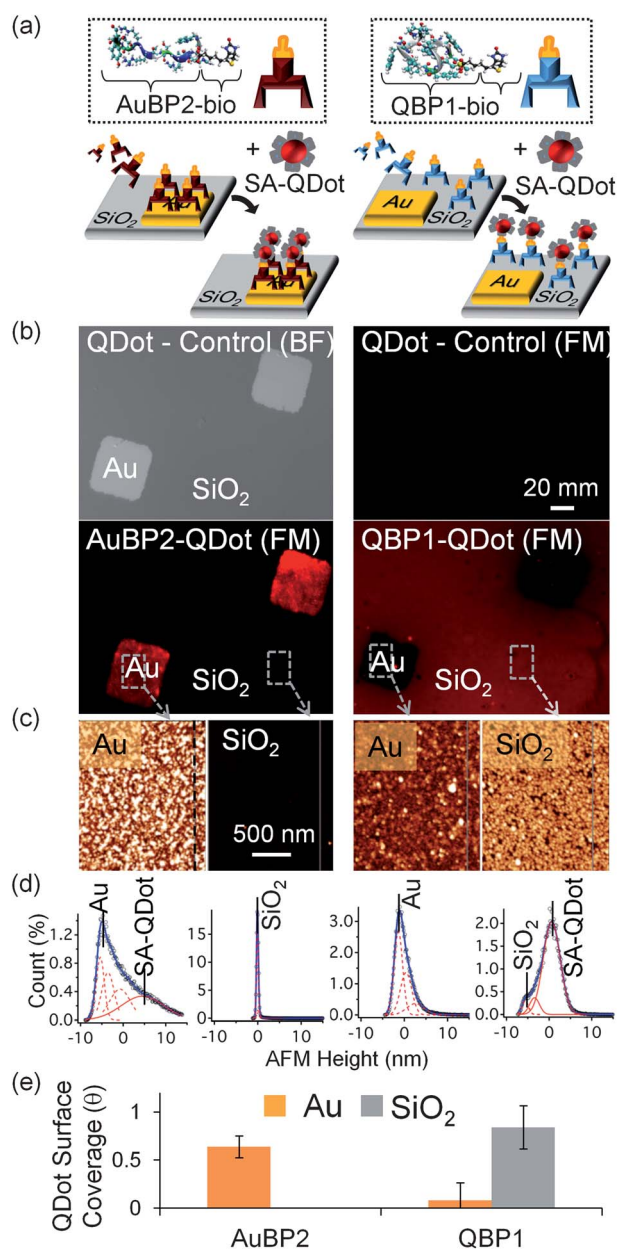
Fig. 3 Peptide-directed immobilization of QDots onto the micro-patterned surface of gold and silica *via* AuBP2 (left) and QBP1 (right). (a) Two-step schematic illustration of multifunctional peptide constructs and peptide-directed immobilization of streptavidin-QDots (SA-QDots) onto gold and silica regions. (b) Bright field (BF) and fluorescence microscopy images (FM) of QDots preferentially immobilized onto gold and silica regions *via* AuBP2 and QBP1, respectively, with control experiments (no peptide present but only SA-QDots alone). (c) AFM topographs of micropatterned surfaces from grey outlined regions in (b) showing AuBP2 on gold micropatterns and QBP1 on silica. (d) Analysis of height distributions from whole AFM images showing histogram peaks representing bare surfaces (analysed in negative controls shown in the ESI†) and additional broader peaks indicating the presence of surface immobilized QDots *via* specific AuBP2 and QBP1. (e) Quantification of QDot surface coverage in images represented in (c) plotted to compare immobilization on gold and silica surfaces *via* AuBP2 and QBP1. Peptide concentration: 20 μM AuBP2-bio and 100 μM QBP1-bio solution in PBS buffer.

SA-functionalized CdSe–ZnS QDots (SA-QDots, Molecular Probes, USA), onto various solid surfaces through combination of peptide material-selectivity characteristics and bio–SA interactions.

Fig. 3a depicts the proposed scheme of targeted QDot immobilization *via* AuBP2 and QBP1 onto either gold pads or the silica regions, respectively, of patterned multimaterial gold/silica surfaces. The regions of peptide-directed QDot assembly would appear red through the formed AuBP-bio/SA-QDot linkage and fluorescent light emission of QDots.[35] As demonstrated in FM images in Fig. 3b, both tested peptide sequences successfully target QDots onto either Au pads or SiO_2 surfaces, respectively. Control experiments carried out using either SA-QDots without the biotinylated peptides or SA-QDots and biotin without the peptides revealed that there is no direct SA-QDot binding on either Au or the SiO_2 wafer itself (shown in the ESI†).

We substantiated the selective behavior of peptides further by imaging the regions of the gold pad and silica substrate using high resolution atomic force microscopy (AFM). Using height distributions from AFM images, shown in Fig. 3e, the selective immobilization of SA-QDot nanostructures onto Au and SiO_2 regions could be quantified *via* surface coverage. Specifically, SA-QDot immobilization is manifested as an additional broad peak at higher height values when compared to characteristic histograms observed for bare Au and SiO_2. This is clearly seen in SA-QDots bound to gold (Fig. 3d, left) where the first three fitted peaks are characteristic of the bare gold (dotted red curves, see also ESI†), while an additional broad peak represents the surface immobilized QDots (solid red curve). The QDot surface coverage
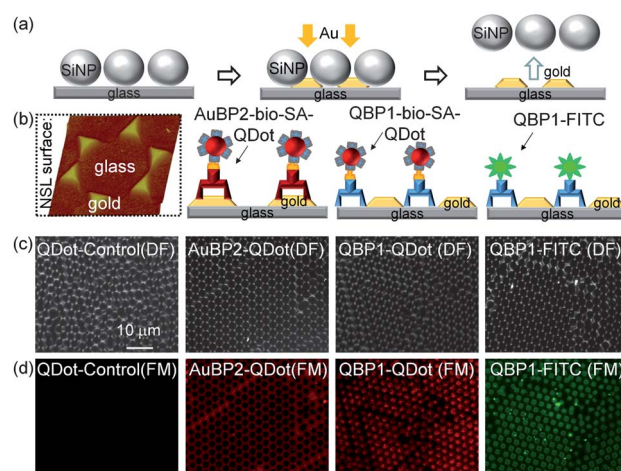

Fig. 4 Peptide-directed immobilization of QDots and FITC on NSL surfaces *via* AuBP2 and QBP1. (a) Schematic of NSL surface fabrication. (b) AFM image of prepared NSL substrate and schematic illustration of peptide-directed specific immobilization of SA-QDots or FITC onto either gold/silica glass. (c and d) Dark field (DF) and corresponding fluorescence images (FM) of the control experiments (no peptide but containing SA-QDots) and directed QDot and FITC immobilization on gold and glass regions *via* the gold-binding (AuBP2-bio) and the silica-binding (QBP1-bio and QBP1-FITC) peptides, respectively. The NSL substrates were prepared by 5 μm bead mask (see ESI† for NSL prepared by 1.5 μm beads used as mask). Peptide concentration: 20 μM AuBP2-bio, 100 μM QBP1-bio and 60 μM QBP1-FITC solution in PBS buffer.
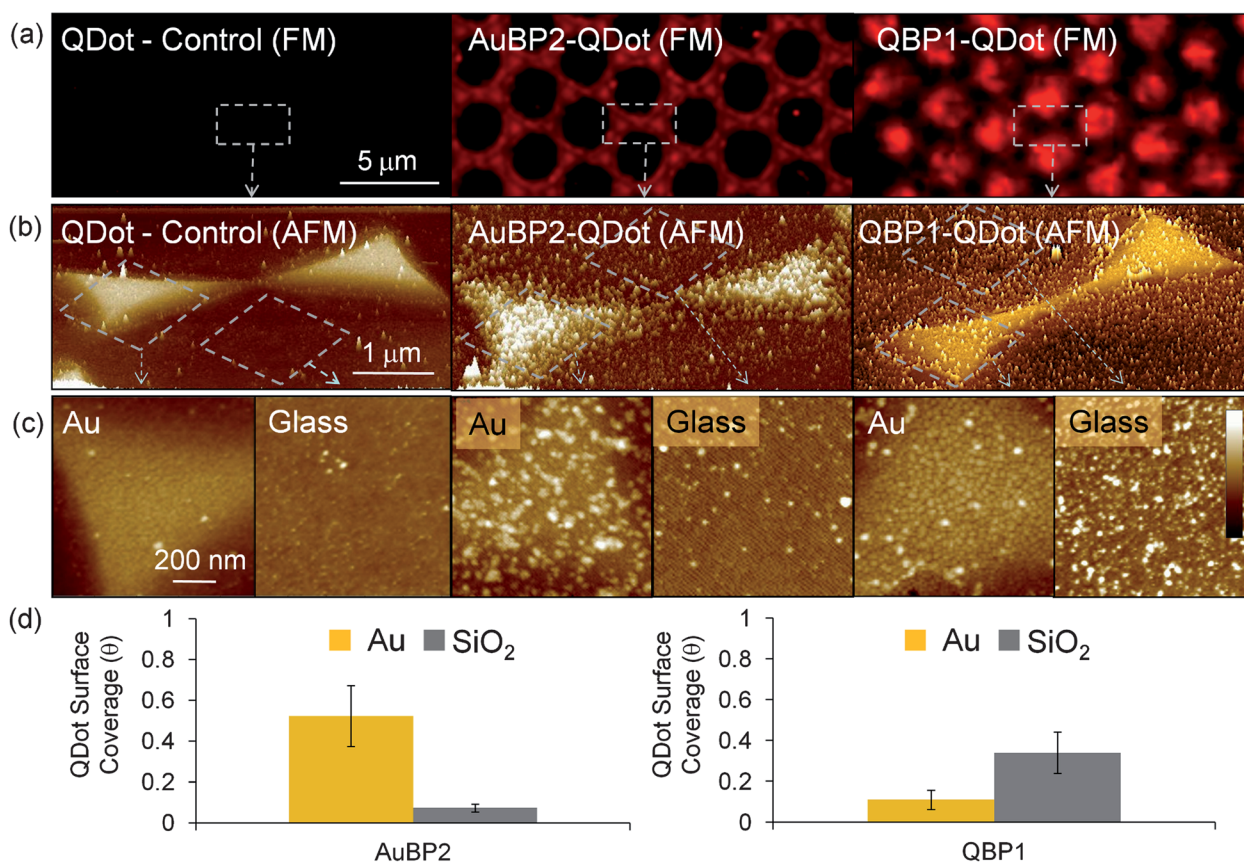
Fig. 5 FM and high resolution AFM and quantification of functionalized NSL surfaces. (a) Magnified fluorescence images of NSL surfaces from Fig. 4, with areas scanned by AFM denoted by grey rectangles. (b) AFM topographs of NSL surfaces from grey outlined regions in (a) showing control, AuBP2-bio-QDots on gold nanostructures and QBP1-bio-QDots on glass from left to right. (c) Further magnified regions denoted by black boxes in (b) showing the specific morphology of individual peptide-QDot conjugates immobilized on their respective material surfaces noted in the corner of the images. Color scale shown in the right-hand image is representative for all AFM images, where white represents 30 nm and black is 0 nm. (d) Quantification of QDot coverage from images represented by row (c) plotted to compare immobilization on gold and glass *via* AuBP2 and QBP1.

(θ) calculated using the area under corresponding QDot peaks in Fig. 3f exhibits a significant increase in the peptide-targeted cases (*i.e.*, AuBP2 on gold, QBP1 on glass). The height distributions of surface immobilized SA-QDot particles, ~5–10 nm from the bare surface, are in agreement with the literature values and, thus, indicate that QDots exist as a single layer.[47]

To further substantiate the applicability of engineered peptides as alternative bio-linkers, we next carried out directed immobilization of SA-QDots and FITC molecules using material-specific peptides on substrates prepared by nanosphere lithography (NSL). The technique of NSL is recognized as an easy, rapid and cost-effective approach in producing a variety of patterned substrates at the micrometre, and even at the 10s of nanometre, dimensions. The technique has been successfully demonstrated in chemical- and bio-sensor applications based on the localized surface plasmon resonance (LSPR) phenomenon.[37]

Control experiments (SA-QDots only) on the NSL patterned substrates (prepared by 5 μm diameter bead masks) showed that the QDots alone do not have any affinity to either of the materials, *i.e.*, silica glass or Au (Fig. 4b) respectively. In contrast, the FM images, recorded following the process of parallel incubation with AuBP2-bio and QBP1-bio followed by SA-QDot incubation (Fig. 4b), demonstrate that both tested solid-binding

peptides, AuBP2 and QBP1, can direct immobilization of QDots onto the respective inorganic patterns of the NSL prepared substrates. Moreover, we found that peptide-directed immobilization of the QDots is possible on even smaller metal regions of the NSL substrates prepared by 1.5 μm bead masks (data shown in the ESI†). Similarly, we also illustrate that the bifunctional QBP1-FITC conjugate specifically binds to the glass region using identical NSL pattern surfaces, as illustrated in Fig. 4.

The plasmonic properties of metal nanostructures are known to affect fluorescent emission intensity of molecular fluorophores when in close proximity to metallic surfaces.[48–50] Thus we scanned various regions of the NSL surface using high resolution non-contact atomic force microscopy (AFM) in order to further investigate and quantify the immobilized QDots on the metal pad and the glass surface. As shown in Fig. 5, AFM scans are in agreement with obtained FM images and show that the QDots preferentially immobilize onto Au or silica regions *via* respective material-selective peptides. Furthermore, when QDot coverage is measured from three 1 μm² AFM images of gold and silica (see Materials and methods), a large increase in QDot surface coverage is observed for the peptide-targeted surfaces. In other words, the coverage of QDots bound to gold *via* AuBP2 is ~10 times higher than on silica and, similarly, ~3 times more QDots

were bound to silica by using QBP1. Due to the probable shadowing by the microspheres during sputter coating and, therefore, broadening of the gold–silica interface region, the data sampling was carried out only from a 1 μm² center of each of the respective regions (*i.e.*, Au and silica) to isolate interference of the transition region at the interface.

Having demonstrated the targeted immobilization of QDots and molecular probes onto their desired materials in parallel experiments (Fig. 4 and 5), the next experimental challenge in this research was to accomplish immobilization of both the QDots and the fluorescein molecules on the same patterned sample simultaneously. The offset fluorescence emission wavelength of QDots605 and FITC enable their simultaneous detection with a proper filter setup in the fluorescence microscope. We first directly immobilized AuBP2-bio onto the Au regions of the gold patterned glass substrate, which was then followed by incubation

with SA-QDot in a stepwise fashion. In the second stage, we exposed the same NSL substrate to the QBP1-FITC molecular construct for directed immobilization on the exposed silica regions (as schematically illustrated in Fig. 6a). The FM and combined overlay images in Fig. 6b reveal both red and green regions that demonstrate the co-assembly of two nanophotonic entities, *i.e.*, QDots and FITC. Taking advantage of the material-specific capabilities of solid-binding peptides, these results clearly demonstrate that two fundamentally different nanoinorganic and molecular species, *i.e.*, QDots and fluorescein molecules, can be specifically targeted towards micron-scale materials (gold and silica, respectively) that are on the same solid substrate. The directed co-assembly enabled by material-specific peptides is a significant result that can now potentially be utilized as the basis for implementations in complex nano- and micro-patterned multimaterial systems for a variety of applications that require, for example, multiple probes for multi-target detection.
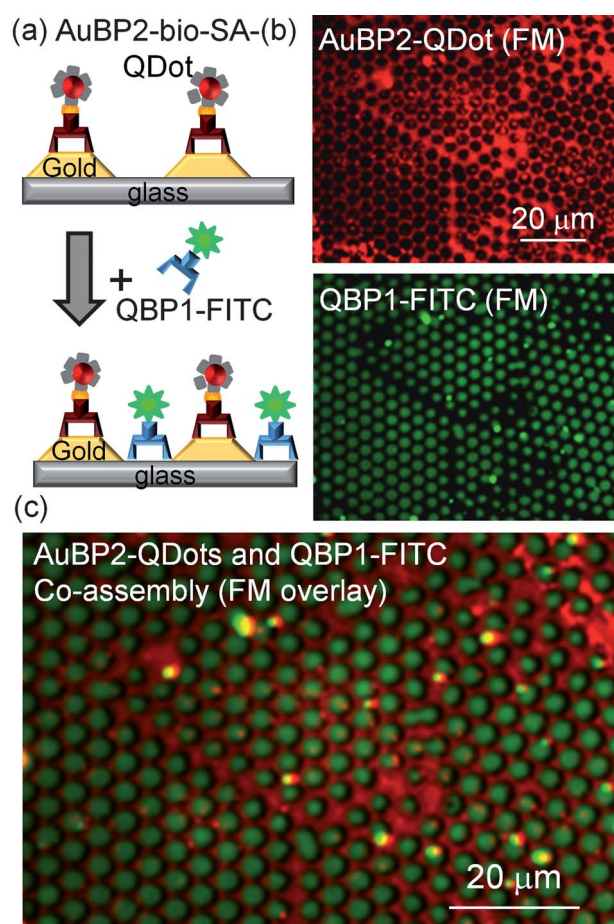
Conclusions

In summary, we demonstrate here, for the first time, the utility of engineered solid-binding peptides as material-specific linkers for simultaneous co-assembly of QDots and fluorescent probe molecules on multimaterial patterned substrates. We have shown that engineered peptide-based linkers can provide both desired multifunctionality and versatility and, thus, direct the immobilization of functional molecules and nanoparticles onto solid surfaces. Solid-binding peptides, moreover, offer unique features that are potentially significant in practical applications that require vigorous control at bio/nano-interfaces: (i) peptides are robust and can be genetically engineered or chemically modified for tailored multifunctionality; (ii) engineered peptides can selectively bind to inorganic targets or onto the desired locations of multi-component patterned substrates; (iii) the nanomaterial assembly processes are carried out under ambient conditions in aqueous solutions, providing a biologically friendly environment, desirable for bionanotechnological applications. The described bio-enabled co-assembly process could be of unique utility in targeted linking and hierarchical assembly of multiple nano- and micro-entities such as nanoparticles, quantum dots, functional synthetic (*e.g.*, fluorescent probes) or biological molecules (*e.g.*, enzymes, other functional proteins, and protein, viral, and cell (*e.g.*, cancer) probes, DNA, RNA, and peptidoglycans), and single-celled organisms (viruses, bacteria, and cells) onto spatially controlled specific locations of complex multimaterial substrates as a novel platform for a wide range of applications in nanophotonics, proteomics, single cell studies, and biosensing devices.

Fig. 6 Simultaneous peptide-directed co-assembly of QDots and FITC fluorophore on the NSL substrate. (a) Schematic illustration of the simultaneous immobilization process using two peptide constructs. (b) Fluorescence images of the SA-QDot immobilized *via* gold-binding peptide (AuBP2-bio) onto gold and the QBP1-FITC construct immobilized onto silica glass. (c) The overlay of the fluorescence images is shown in the bottom revealing that the FITC molecules (attached to QBP1) are immobilized on the circular regions of the silica and the QDots are immobilized onto the gold triangular island nanostructures *via* AuBP2-bio. The peptide concentrations are the same as in Fig. 1 and 2. DF and fluorescence images of control experiments are shown in Fig. 4.

Facilities), a member of the MRFN (Materials Research Facilities Network).

References

1 C. A. Mirkin, R. L. Letsinger, R. C. Mucic and J. J. Storhoff, *Nature*, 1996, **382**, 607–609.
2 N. Nath and A. Chilkoti, *Anal. Chem.*, 2004, **76**, 5370–5378.
3 T. Endo, K. Kerman, N. Nagatani, Y. Takamura and E. Tamiya, *Anal. Chem.*, 2005, **77**, 6976–6984.
4 H. Matsui, P. Porrata and G. E. Douberly, *Nano Lett.*, 2001, **1**, 461–464.
5 J. M. Bingham, K. A. Willets, N. C. Shah, D. Q. Andrews and R. P. Van Duyne, *J. Phys. Chem. C*, 2009, **113**, 16839–16842.
6 D. Qin, Y. N. Xia and G. M. Whitesides, *Nat. Protoc.*, 2010, **5**, 491–502.
7 B. D. Ratner, *J. Mol. Recognit.*, 1996, **9**, 617–625.
8 U. Reineke, R. Volkmer-Engert and J. Schneider-Mergener, *Curr. Opin. Biotechnol.*, 2001, **12**, 59–64.
9 M. D. Porter, T. B. Bright, D. L. Allara and C. E. D. Chidsey, *J. Am. Chem. Soc.*, 1987, **109**, 3559–3568.
10 M. Mrksich and G. M. Whitesides, *Annu. Rev. Biophys. Biomol. Struct.*, 1996, **25**, 55–78.
11 J. B. Brzoska, I. Benazouz and F. Rondelez, *Langmuir*, 1994, **10**, 4367–4373.
12 Z. Y. Li, S. C. Chang and R. S. Williams, *Langmuir*, 2003, **19**, 6744–6749.
13 P. Fenter, P. Eisenberger, J. Li, N. Camillone, S. Bernasek, G. Scoles, T. A. Ramanarayanan and K. S. Liang, *Langmuir*, 1991, **7**, 2013–2016.
14 G. MacBeath and S. L. Schreiber, *Science*, 2000, **289**, 1760–1763.
15 P. E. Laibinis, G. M. Whitesides, D. L. Allara, Y. T. Tao, A. N. Parikh and R. G. Nuzzo, *J. Am. Chem. Soc.*, 1991, **113**, 7152–7167.
16 G. L. Zhen, D. Falconnet, E. Kuennemann, J. Voros, N. D. Spencer, M. Textor and S. Zurcher, *Adv. Funct. Mater.*, 2006, **16**, 243–251.
17 M. Sarikaya, C. Tamerler, A. K. Y. Jen, K. Schulten and F. Baneyx, *Nat. Mater.*, 2003, **2**, 577–585.
18 C. Tamerler, D. Khatayevich, M. Gungormus, T. Kacar, E. E. Oren, M. Hnilova and M. Sarikaya, *Biopolymers*, 2010, **94**, 78–94.
19 T. Kacar, M. T. Zin, C. So, B. Wilson, H. Ma, N. Gul-Karaguler, A. K. Y. Jen, M. Sarikaya and C. Tamerler, *Biotechnol. Bioeng.*, 2009, **103**, 696–705.
20 S. R. Whaley, D. S. English, E. L. Hu, P. F. Barbara and A. M. Belcher, *Nature*, 2000, **405**, 665–668.
21 R. R. Naik, S. J. Stringer, G. Agarwal, S. E. Jones and M. O. Stone, *Nat. Mater.*, 2002, **1**, 169–172.
22 G. P. Smith, *Science*, 1985, **228**, 1315–1317.
23 E. T. Boder and K. D. Wittrup, *Nat. Biotechnol.*, 1997, **15**, 553–557.
24 S. Brown, *Nat. Biotechnol.*, 1997, **15**, 269–272.
25 M. Hnilova, E. E. Oren, U. O. S. Seker, B. R. Wilson, S. Collino, J. S. Evans, C. Tamerler and M. Sarikaya, *Langmuir*, 2008, **24**, 12440–12445.
26 Y. Huang, C. Y. Chiang, S. K. Lee, Y. Gao, E. L. Hu, J. De Yoreo and A. M. Belcher, *Nano Lett.*, 2005, **5**, 1429–1434.
27 U. O. S. Seker, B. Wilson, S. Dincer, I. W. Kim, E. E. Oren, J. S. Evans, C. Tamerler and M. Sarikaya, *Langmuir*, 2007, **23**, 7895–7900.
28 C. K. Thai, H. X. Dai, M. S. R. Sastry, M. Sarikaya, D. T. Schwartz and F. Baneyx, *Biotechnol. Bioeng.*, 2004, **87**, 129–137.
29 K. Shiba, *Curr. Opin. Biotechnol.*, 2010, **21**, 412–425.
30 E. E. Oren, C. Tamerler, D. Sahin, M. Hnilova, U. O. S. Seker, M. Sarikaya and R. Samudrala, *Bioinformatics*, 2007, **23**, 2816–2822.
31 J. M. Slocik and R. R. Naik, *Chem. Soc. Rev.*, 2010, **39**, 3454–3463.
32 S. Brown, M. Sarikaya and E. Johnson, *J. Mol. Biol.*, 2000, **299**, 725–735.
33 W. Zhou, D. T. Schwartz and F. Baneyx, *J. Am. Chem. Soc.*, 2010, **132**, 4731–4738.
34 H. X. Dai, W. S. Choe, C. K. Thai, M. Sarikaya, B. A. Traxler, F. Baneyx and D. T. Schwartz, *J. Am. Chem. Soc.*, 2005, **127**, 15637–15643.
35 C. Tamerler, M. Duman, E. E. Oren, M. Gungormus, X. R. Xiong, T. Kacar, B. A. Parviz and M. Sarikaya, *Small*, 2006, **2**, 1372–1378.
36 Z. J. Lu, K. S. Murray, V. Vancleave, E. R. Lavallie, M. L. Stahl and J. M. McCoy, *Bio Tech.*, 1995, **13**, 366–372.
37 A. J. Haes, S. L. Zou, G. C. Schatz and R. P. Van Duyne, *J. Phys. Chem. B*, 2004, **108**, 109–116.
38 T. Kacar, J. Ray, M. Gungormus, E. E. Oren, C. Tamerler and M. Sarikaya, *Adv. Mater.*, 2009, **21**, 295–299.
39 C. Tamerler, E. E. Oren, M. Duman, E. Venkatasubramanian and M. Sarikaya, *Langmuir*, 2006, **22**, 7712–7718.
40 E. E. Oren, R. Notman, I. W. Kim, J. S. Evans, T. R. Walsh, R. Samudrala, C. Tamerler and M. Sarikaya, *Langmuir*, 2010, **26**, 11003–11009.
41 M. Hoefling, F. Iori, S. Corni and K. E. Gottschalk, *Langmuir*, 2010, **26**, 8347–8351.
42 J. Kim, Y. Rheem, B. Yoo, Y. Chong, K. N. Bozhilov, D. Kim, M. J. Sadowsky, H. G. Hur and N. V. Myung, *Acta Biomater.*, 2010, **6**, 2681–2689.
43 Y. N. Tan, J. Y. Lee and D. I. C. Wang, *J. Am. Chem. Soc.*, 2010, **132**, 5677–5686.
44 F. Rusmini, Z. Y. Zhong and J. Feijen, *Biomacromolecules*, 2007, **8**, 1775–1789.
45 M. T. Kumara, B. C. Tripp and S. Muralidharan, *Chem. Mater.*, 2007, **19**, 2056–2064.
46 P. C. Weber, D. H. Ohlendorf, J. J. Wendoloski and F. R. Salemme, *Science*, 1989, **243**, 85–88.
47 H. Bui, C. Onodera, C. Kidwell, Y. Tan, E. Graugnard, W. Kuang, J. Lee, W. B. Knowlton, B. Yurke and W. L. Hughes, *Nano Lett.*, 2010, **10**, 3367–3372.
48 R. M. Bakker, H. K. Yuan, Z. T. Liu, V. P. Drachev, A. V. Kildishev, V. M. Shalaev, R. H. Pedersen, S. Gresillon and A. Boltasseva, *Appl. Phys. Lett.*, 2008, **92**, 043101.
49 Y. Chen, K. Munechika and D. S. Ginger, *Nano Lett.*, 2007, **7**, 690–696.
50 K. Leong, Y. C. Chen, D. J. Masiello, M. T. Zin, M. Hnilova, H. Ma, C. Tamerler, M. Sarikaya, D. S. Ginger and A. K. Y. Jen, *Adv. Funct. Mater.*, 2010, **20**, 2675–2682.